The interplay of tunneling, resonance, and dissipation in quantum barrier crossing: A numerical study

Yoshitaka Tanimura[a] and Peter G. Wolynes
Beckman Institute and School of Chemical Sciences, University of Illinois at Urbana-Champaign, Urbana, Illinois 61801

We discuss the interplay of various quantum effects on barrier crossing for a one-dimensional system with dissipation. This is based on a numerical study using a hierarchy of kinetic equations introduced by Tanimura and Kubo. The numerical work uses a grid in phase space for the Wigner distribution and deals with both the classical limit and the tunneling regimes.

I. INTRODUCTION

The study of the effect of a dissipative environment on barrier crossing in the classical and quantum regimes has been a central concern of theoretical chemical physicists in the last decade. Numerous insights have been obtained from the interplay of qualitative arguments, quantitative analytical calculations, and experiments, and for the classical systems, definitive numerical studies.[1] As far as numerical work goes, the quantum case presents some problems. Quantum activated events, in the absence of dissipation, can be easily studied by a wide variety of numerical methods based on wave functions.[2] When dissipation is important, wave-function-based methods are not appropriate since dissipation requires the presence of many degrees of freedom. Integrating out degrees of freedom is most naturally done in the path integral formulation of quantum mechanics, where it leads to influence functionals.[3–5] The resulting path integrals are highly coupled and many dimensional, thus grid-based methods do not work very well for evaluating these integrals because of the infamous crisis of dimensionality.[6] One is forced to examine the Monte Carlo approaches.[7–10] Monte Carlo methods work best when the integrand is of one sign or has only weak oscillations about zero. Fortunately, it turns out that the tunneling aspects of chemical rate phenomena can be treated largely with imaginary time path integrals which have positive integrands. A variety of successes in determining the tunneling aspects of chemical reaction dynamics can be cited, ranging from systems as simple as schematic double well potentials[9,10] through H + H$_2$,[7] all the way to the electron transfer reactions of inorganic complexes in water[11,12] and biological macromolecules.[8,13] These studies, however, focus on only one of the quantum aspects of activated events. A complete picture of reaction dynamics must deal with phenomena that can only be described easily in real time.

Qualitative arguments about rates suggest that such effects as energy diffusion and quantum interference effects such as resonance may be important in some regimes for quantum activated events. None of these effects are captured adequately by imaginary time methods. A great deal of effort

has, therefore, been expended on trying to evaluate numerically path integrals in real time.[14–17] Here, straightforward Monte Carlo methods become problematic because of the oscillating phases of wave functions. Attempts to ameliorate this problem via stationary phase methods and nonrandom sampling methods have been moderately successful, but in all likelihood, do not solve the problem in general. In any event, at the moment these methods are so computationally costly that they have not given a complete picture of the role of dissipative environments on quantum activated events in all regimes.

An alternative, but perhaps even more venerable approach to integrating out degrees of freedom leads to a description in terms of equations of motions for reduced density matrices. These equations are entirely analogous to the classical kinetic equations which proved to be useful for classical barrier crossing. Indeed, from the earliest days, they have been used to describe some features of quantum barrier crossing.[18] They have been limited by two features, however. First, equations of motion for the reduced density matrix were originally applicable and derivable only in the weak coupling to the bath. Because of this, they took into account none of the important effects that were first seen through imaginary time path integral methods, such as the change of the equilibrium probability densities through dissipative coupling. Second, the reduced density matrix equations are, per force, of twice the dimensionality of the time-dependent Schrödinger equation. Thus, until the advent of fast computers, grid-based methods for their solution were too difficult, even in the case of one-dimensional problems with dissipation.

The advent of fast computational methods and fast computers has led to a reexamination of quantum kinetic equations as an approach to quantum dynamics of low-dimensional systems. Bull[19] has studied the quantum Fokker–Planck equation for a hindered rotor, determining the correlation functions of relevance to nuclear magnetic resonance (NMR). Jean, Fleming, and Friesner[20] have studied the multilevel Redfield equations appropriate to a curve crossing problem modeling the initial events of photosynthesis. These studies have been limited to the strict weak coupling regime. In 1989, Tanimura and Kubo[21] showed how one could obtain a hierarchy of kinetic equations for reduced

[a] Present address: Department of Chemistry, University of Rochester, Rochester, NY 14627.

density matrices that was valid in the strong coupling regime. Physically, one can think of this hierarchy of equations as dealing with a set of density matrices modeling the states of the system with various numbers of phonons excited in the bath. In this respect, the method has much in common with the recent work of Makri[22] which has been implemented for finite-dimensional heat baths. Tanimura and Wolynes[23] showed how this hierarchy of kinetic equations could be solved numerically on a grid and illustrated with calculations on harmonic oscillators, as well as one representative calculation on a double well system.

In this paper, we present a more complete study of the various regimes of quantum barrier crossing using the quantum kinetic equations. The present numerical study allows one to demonstrate many of the features of the interplay among tunneling, resonance, and dissipation in barrier crossing. Individually, many of the aspects have been discussed from a qualitative viewpoint (Ref. 1). For example, it is now understood that tunneling becomes more important at low temperature—that it is diminished through the effects of dissipation. It is also widely believed that resonance effects can be smeared out by dissipation and that resonance effects have an interesting interplay with the energy activation events.[1(b)] The numerical studies here show all of these qualitative features and their interaction. These results are displayed in a three-dimensional plot of rate constant vs dissipation and temperature which generalizes the extremely familiar rate coefficient vs friction curves used in discussing classical barrier crossing.

The organization of this paper is as follows: In Sec. II, the Fokker–Planck equations and the hierarchy equations are summarized and the numerical aspects of studying the Wigner function representation of a quantal density operator are described. Second, the methodology of obtaining rate coefficients is explained in some detail. In Sec. III, the numerical results are presented for activation and tunneling in a cosinusoidal potential, and the Kramers turnover curves for classical and quantum cases are presented, both for a white noise heat bath and for a Gaussian–Markovian heat bath. Finally, in the last section, the strength and weakness of kinetic equation approaches are discussed briefly.

II. METHODOLOGY

A. The quantum Fokker–Planck equation for a Gaussian–Markovian bath

In our previous work (Ref. 23, Tanimura and Wolynes, hereafter TW), we derived the quantum Fokker–Planck equation for the Gaussian–Markovian colored-noise bath. Here we summarize briefly the previous results. Let us consider a reaction system S (inertial mass I, coordinate $\hat{\theta}$, and momentum $\hat{P}$) moving in a potential $U(\hat{\theta})$ and interacting linearly with the harmonic oscillators bath B (mass m_j, coordinate $\hat{x}_j$, and momentum $\hat{p}_j$). The Hamiltonian with the counterterm is[4]

$$H_{S+B} = \frac{\hat{P}^2}{2I} + U(\hat{\theta})$$
$$+ \sum_j \left[\frac{\hat{p}_j^2}{2m_j} + \frac{m_j \omega_j^2}{2} \left(\hat{x}_j - \frac{c_j \hat{\theta}}{m_j \omega_j^2} \right)^2 \right]. \quad (1)$$

All information about the bath is specified by the spectral density

$$J(\omega) = \hbar\omega \sum_j \left(\frac{c_j^2}{4m_j \omega_j^2} \right) [\delta(\omega - \omega_j) + \delta(\omega + \omega_j)] \quad (2)$$

and the initial temperature of the bath $k_B T = 1/\beta$. Here we assume the Ohmic dissipation with the Lorentzian cutoff

$$J(\omega) = \frac{\hbar I \zeta}{2\pi} \frac{\omega\gamma^2}{\gamma^2 + \omega^2}, \quad (3)$$

where ζ is the zero frequency friction and γ is a relaxation time for the bath. With the assumption of the high temperature bath $\beta\hbar\gamma \ll 1$, this spectral density produces exponentially correlated noise $\langle \Omega(t)\Omega(t') \rangle \propto \exp[-\gamma(t - t')]$, where $\Omega(t)$ represents the noise produced by the bath. Since the bath of harmonic oscillators has the character of the Gaussian, thus the bath system considered here is Gaussian–Markovian. The Markovian property is produced not only by the delta-correlated noise, but also the exponentially correlated noise.[24] As shown in TW, the equation of motion for the Hamiltonian equation (1) with Eq. (3) at the high temperature bath $\beta\hbar\gamma \ll 1$ is expressed in the operator form as

$$\frac{\partial}{\partial t} \hat{\rho}_0(t) = -\frac{i}{\hbar} H_0^\times \hat{\rho}_0(t) - \frac{i}{\hbar} \hat{\theta}^\times \hat{\rho}_1(t), \quad (4)$$

$$\frac{\partial}{\partial t} \hat{\rho}_n(t) = -\left(\frac{i}{\hbar} H_0^\times + n\gamma \right) \hat{\rho}_n(t) - \frac{i}{\hbar} \hat{\theta}^\times \hat{\rho}_{n+1}(t)$$
$$- \frac{ni}{\hbar} \Theta_F \hat{\rho}_{n-1}(t), \quad (n \geqslant 1) \quad (5)$$

and to truncate the hierarchy for the deepest level

$$\frac{\partial}{\partial t} \hat{\rho}_N(t) = -\left(\frac{i}{\hbar} H_0^\times + N\gamma \right) \hat{\rho}_N(t) - \frac{1}{\gamma\hbar^2} \hat{\theta}^\times \Theta_F \hat{\rho}_N(t)$$
$$- \frac{Ni}{\hbar} \Theta_F \hat{\rho}_{N-1}(t), \quad (6)$$

for $N\gamma \gg \omega_0$, where ω_0 is the characteristic frequency of the reaction system. In the above,

$$H_0 = \left(\frac{\hat{P}^2}{2I} + U(\hat{\theta}) \right), \quad \Theta_F = \frac{\hbar\zeta\gamma}{2} \left(i\hat{P}^\circ + \frac{2I}{\beta\hbar} \hat{\theta}^\times \right) \quad (7)$$

with the hyperoperators

$$\hat{A}^\times \hat{B} = \hat{A}\hat{B} - \hat{B}\hat{A}, \quad \hat{A}^\circ \hat{B} = \hat{A}\hat{B} + \hat{B}\hat{A}, \quad (8)$$

for any operators $\hat{A}$ and $\hat{B}$, respectively. The hierarchical elements $\hat{\rho}_n$ represent the n phonon dressed state with the decay rate $n\gamma$ and the conventional density operator $\hat{\rho}$ corresponds to $\hat{\rho}_0$. Each equation in Eqs. (4)–(6), e.g., for $\hat{\rho}_n$, represents the rate law among the three elements $\hat{\rho}_n, \hat{\rho}_{n-1}$, and $\hat{\rho}_{n+1}$, namely the time evolution of $\hat{\rho}_n$ is determined by its time evolution $(i/\hbar)H_0^\times + n\gamma$ and the incoming and outgoing contribution from $\hat{\rho}_{n-1}$ and $\hat{\rho}_{n+1}$. Because of this hierarchical structure, we may deal with the strong system–bath interactions.

Here, we should also mention that correlated initial conditions play an important role for the colored noise or the strong system–bath interaction case. Let us denote the total Hamiltonian as $H = H_0 + H_I + H_B$, where H_0, H_B, and H_I represent the Hamiltonian of S, B, and these interactions,

respectively. To obtain the conventional quantum Fokker–Planck equation,[25] or equivalently the quantum master equation,[24] one usually uses the factorized assumption $\hat{\rho}_{S+B}(t_i) = \exp(-\beta H_B)\hat{\rho}(t_i)$, where $\hat{\rho}(t_i)$ is the density operator of S. In this chemical reaction problem, the initial condition for the total system is assumed to be the equilibrium one $\hat{\rho}_{S+B}(t_i) = \exp[-\beta(H_0 + H_I + H_B)]$, however, the equilibrium state we can define for the conventional quantum Fokker–Planck equation based on the white noise is $\hat{\rho}_{S+B}(t_i) = \exp(-\beta H_B)\exp(-\beta H_0)$ because of the factorization assumption. The differences between the true equilibrium state and the factorized one are the terms such as $\beta H_I \exp[-\beta(H_0 + H_B)]$, $\beta^2 \exp[-\beta(H_0 + H_B)]$ $H_I H_I$, etc. The initial conditions taking into account these terms are sometimes called correlated initial conditions. We may neglect correlated terms for the white noise case, where the factorization assumption works well, but we must take them into account for the strong interaction or the correlated noise case. In our approach, these terms are expressed by using the hierarchal elements $\hat{\rho}_1, \hat{\rho}_2$, etc. The true equilibrium state can be obtained by continuing the calculation until all elements $\hat{\rho}_n$ reach steady state. Then using these elements as the initial conditions $\hat{\rho}_n(t_i)$ defines the correlated equilibrium initial condition.

In TW, we demonstrated the calculation using the coordinate representation of the density matrix, however, here we use the Wigner function based on the phase space to study the tunneling effects. The relationship between the quantal density operator and phase space distribution such as that of classical mechanics is obtained from the Wigner transformation, which is presented in the form[26]

$$W(P,\theta;t) = \frac{1}{2\pi\hbar}\int_{-\infty}^{\infty} e^{iP\theta'/\hbar}$$
$$\times \langle\theta - \theta'/2|\hat{\rho}(t)|\theta + \theta'/2\rangle d\theta'. \quad (9)$$

The rule is that all operators consisting of $\hat{P}$ and $\hat{\theta}$ have to be replaced according to[27]

$$A(\hat{P},\hat{\theta})\hat{\rho}(t) \to A\left(P + \frac{\hbar}{2i}\frac{\partial}{\partial\theta},\ \theta - \frac{\hbar}{2i}\frac{\partial}{\partial P}\right)W(P,\theta;t),$$

$$\hat{\rho}(t)A(\hat{P},\hat{\theta}) \to A\left(P - \frac{\hbar}{2i}\frac{\partial}{\partial\theta},\ \theta + \frac{\hbar}{2i}\frac{\partial}{\partial P}W(P,\theta;t)\right),$$
$$(10)$$

where $A(\hat{P},\hat{\theta})$ is any operator of $\hat{P}$ and $\hat{\theta}$. Then Eqs. (4)–(6) are replaced by

$$\frac{\partial}{\partial t}W_0 = -\hat{L}_{QM}W_0 + \partial_P W_1, \quad (11)$$

$$\frac{\partial}{\partial t}W_n = -(\hat{L}_{QM} + n\gamma)W_n + \partial_P W_{n+1} + n\Theta_F(P)W_{n-1}$$
$$(n \geqslant 1), \quad (12)$$

and

$$\frac{\partial}{\partial t}W_N = -(\hat{L}_{QM} + N\gamma)W_N + \frac{1}{\gamma}\partial_P\Theta_F(P)W_N$$
$$+ N\Theta_F(P)W_{N-1} \quad (13)$$

for the Wigner function $W_n \equiv W_n(P,\theta;t)$. Here,

$$\partial_P = \frac{\partial}{\partial P},\quad \Theta_F(P) = \zeta\gamma\left(P + \frac{I}{\beta}\frac{\partial}{\partial P}\right). \quad (14)$$

The quantal Liouvillian for the Wigner function is defined by

$$-\hat{L}_{QM}W = -\frac{P}{I}\frac{\partial W}{\partial\theta} - \frac{1}{\hbar}\int_{-\infty}^{\infty}\frac{dP'}{2\pi\hbar}$$
$$\times V(P - P',\theta)W(P',\theta) \quad (15)$$

with

$$V(P,\theta) = 2\int_0^{\infty}d\theta'\sin(P\theta'/\hbar)$$
$$\times[U(\theta + \theta'/2) - U(\theta - \theta'/2)]. \quad (16)$$

Equation (16) is the Fourier transform representation of the potential term which is convenient for studying the quantum effects (see Ref. 28). Equations (11)–(13) are the quantum Fokker–Planck equations for the Gaussian–Markovian noise bath. This hierarchical equation can be numerically evaluated by using the finite difference expression of the differential operators and the Wigner function.

If we take the classical limit, the Liouvillian equation (15) with Eq. (16) reduces to

$$-\hat{L}_{CM}W = \left[-\frac{P}{I}\frac{\partial}{\partial\theta} + \frac{\partial U(\theta)}{\partial\theta}\frac{\partial}{\partial P}\right]W(P,\theta). \quad (17)$$

The operators given by Eq. (14) are identical in the classical and the quantal cases. Thus, we may obtain the classical Fokker–Planck equation for the Gaussian–Markovian bath simply by replacing $\hat{L}_{QM}$ by $\hat{L}_{CM}$. Although the classical and the quantal equations have similar form, the quantal equation can be applied only for the high temperature system or the long correlated noise because of the limitation $\beta\hbar\gamma \leqslant 1$.

In the white noise limit $\gamma \gg \omega_0$, where ω_0 is the characteristic frequency of the reaction system, we may terminate the hierarchy in Eqs. (11)–(13) by setting $N = 0$, obtaining the quantum Fokker–Planck equation for the Gaussian–white noise bath

$$\frac{\partial}{\partial t}W_0 = -\hat{L}_{QM}W_0 + \zeta\frac{\partial}{\partial P}\left(P + \frac{I}{\beta}\frac{\partial}{\partial P}\right)W_0. \quad (18)$$

Since we have assumed $\beta\hbar\gamma \leqslant 1$, the temperature restriction to the Gaussian-white case [Eq. (18)] is more strict than that for the Gaussian–Markovian case [Eqs. (11)–(13)]. Violation of the limitation $\gamma \gg \omega_0$ with $\beta\hbar\gamma \leqslant 1$ in Eq. (18) may cause unphysical results such as the negative probability $P(\theta) \equiv \int dp\ W(p,\theta) < 0$.[29,30] Note that the low temperature correction of Eq. (18) can be made by using Eqs. (A9) and (A10) of TW. We may also obtain Eq. (18) by assuming the very weak system–bath interaction, since, in this case, the multiple interactions do not play a role and the higher-order hierarchy can be terminated. Thus, we may apply Eq. (18) to the low temperature system if the system–bath interaction is weak enough. In the classical limit, the quantum Fokker–Planck equation for the Gaussian-white bath reduces to the classical Fokker–Planck equation

$$\frac{\partial}{\partial t} W_0 = -\hat{L}_{CL} W_0 + \zeta \frac{\partial}{\partial P}\left(P + \frac{I}{\beta}\frac{\partial}{\partial P}\right) W_0$$

$$= \left[-\frac{P}{I}\frac{\partial}{\partial \theta} + \frac{\partial U(\theta)}{\partial \theta}\frac{\partial}{\partial P}\right] W_0$$

$$+ \zeta \frac{\partial}{\partial P}\left(P + \frac{I}{\beta}\frac{\partial}{\partial P}\right) W_0. \tag{19}$$

The fully classical equation never violates the positivity criterion, if the initial condition does not. In Sec. III, we focus on the Gaussian-white case and discuss secondly the Gaussian–Markovian case since the numerical integration of the quantum Gaussian–Markovian equation using present computers is time consuming and, as shown in TW, the effects in the white noise and Markovian noise cases are qualitatively similar. Although the quantum Fokker–Planck equation for the Gaussian-white bath cannot be applied for the strong system–bath interaction at the low temperature, we may follow up the results in this case by comparing the results from the quantum Fokker–Planck equation for the Gaussian–Markovian bath.

The advantages of using Wigner functions instead of using density elements are the following: first, the phase space description allows us to make direct interpretations of the dynamics. Thus, we may easily discuss the classical and the quantum systems on the same basis. Second, we may suppress the periodic boundary conditions as we will show in Sec. III. Third, numerical calculations are easier. Since the elements of the Wigner function are real, we may save on memory compared with that needed for the complex density elements. In our approach, memory consumption is one of the major limitations for numerical computation, since we must take into account the many-leveled hierarchy for the strong system–bath interaction.

A current limitation of our approach is that it is most easily applied to the Gaussian–Markovian bath. Also the temperature limitation $\beta\hbar\gamma \leqslant 1$ for the quantum system can give problems. There is also a computational limitation. Because we must take into account the many-leveled hierarchy for the strong system–bath case, it is difficult to calculate two- or higher-dimensional systems with today's computers.

B. Numerical-linear-response experiment for activation events

To study the transition between the wells, we computationally carry out a linear response experiment using the Fokker–Planck equations summarized in Sec. II A. Consider, as the simplest possible model of a two state system, the double well potential of Fig. 1, representing the potential $U(\theta)$ corresponding to the rotational motion along the angle θ of the intermolecular degree of freedom. The two internal states L and R are specified by a dividing point $\theta = \pi$ and boundary points $\theta = 0$ and 2π with the periodical boundary condition. Let us denote the population of L and R states as $N_L(t)$ and $N_R(t)$, then the rate law capturing the traditional phenomenology is

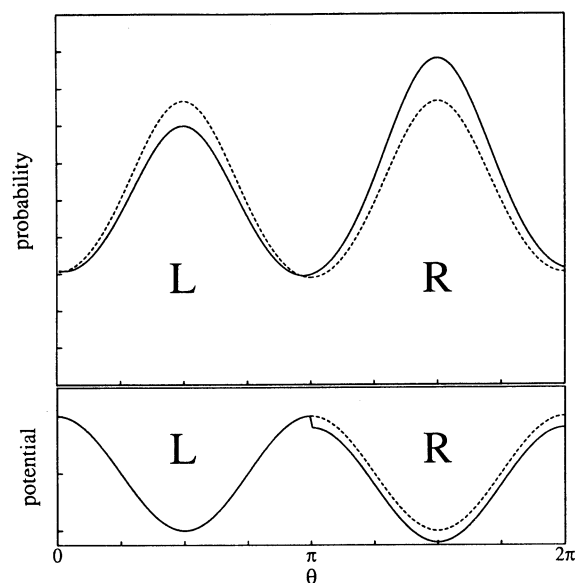$$\frac{dN_L(t)}{dt} = -k_{LR} N_L(t) + k_{RL} N_R(t), \tag{20}$$

FIG. 1. The perturbed (solid line) and unperturbed potentials (dashed line) and corresponding equilibrium states in the quantum case.

where $N_L(t) + N_R(t) = $ const. If $N_L(t) = N^e + \delta N(t)$, where N_e is the equilibrium population, we obtain a simple linear relaxation law for the deviation from equilibrium

$$\frac{d\delta N(t)}{dt} = -k\delta N(t), \tag{21}$$

where $k = k_{LR} + k_{RL}$. We can determine k by taking the ratio

$$k(t) = -\frac{d\delta N(t)/dt}{\delta N(t)} = -\frac{d}{dt}\ln[\delta N(t)], \tag{22}$$

where the second equality can apply only to the case $\delta N(t) > 0$. As is well known, if the traditional phenomenology is correct, there is a plateau regime in which $k(t)$ is essentially constant k_{rxn} and we have

$$\delta N(t) \propto \exp(-k_{rxn}t),$$

for large t. The value of k_{rxn} can be determined by looking at the asymptotic limit of the slope of a semilog plot of $d\delta N(t)/dt$ vs t.

To apply Eq. (22), all that is necessary is to perturb the populations from the equilibrium state. If this perturbation is small enough, $d\delta N(t)/dt$ and $\delta N(t)$ are expected to be proportional to the strength of the perturbation as we will show later in this section and the quantity evaluated from Eq. (22) does not depend on the form of perturbation. So one uses the following perturbation:

$$U(\theta) \to U(\theta) - \epsilon F(\theta) \equiv U(\theta) - \epsilon U_0[S(\theta - \pi)$$

$$- S(\theta - 2\pi)] \quad (0 < \theta \leqslant 2\pi), \tag{23}$$

where $S(\theta)$ is the step function, U_0 is the barrier height, and ϵ is the small constant. The equilibrium distribution functions for the unperturbed and the perturbed potentials are pictured in Fig. 1. By turning on the perturbation for a suffi-

cient time, the system comes to a perturbed equilibrium state. By this perturbation, the population of the left well is shifted to the right well compared with the unperturbed equilibrium state. After the system comes to the perturbed equilibrium state, the perturbation is turned off (this defines time $t = 0$). Now the populations, equilibrated with the perturbation, are no longer in equilibrium and will have to re-equilibrate to those of the unperturbed system. The change of the population in the right well $\delta N(t)$ is now defined by using the density operator as follows:

$$\delta N(t) = \text{Tr}[\hat{\rho}(t)G(\theta)] - \text{Tr}[\hat{\rho}^e G(\theta)], \qquad (24)$$

where

$$G(\theta) = S(\theta - \pi) - S(\theta - 2\pi) \qquad (25)$$

and $\hat{\rho}^e$ is the equilibrium state for the unperturbed Hamiltonian H,

$$\rho^e = e^{-\beta H}/\text{Tr}(e^{-\beta H}). \qquad (26)$$

Thus, by evaluating the time response of the density operator for the perturbation, we may evaluate $k(t)$ from Eq. (22). This is the linear response experiment and we will perform this procedure numerically in Sec. III using the kinetic equation explained in Sec. II A. Although this is a cumbersome procedure, it is necessary for making contact with the experimentally observable rate constant. The rate constant applies to a long-time steady-state situation and it requires dynamics from a correctly equilibrated state in which the bath is correlated quantum mechanically with the reaction system. The density state at $t = 0$ can be regarded as the correlated initial condition discussed in Sec. II A.

This linear response analysis is the basis of all correlation function formulas for relaxation rates.[31–33] Here we discuss some details. For a low barrier potential, it may be difficult to separate the "molecular" from the reaction time scale. However, for high barrier, the change of $\delta N(t)$ is small at short time and we may set $\delta N(t) \approx \delta N(0)$. Then, by performing the Kubo transformation, the relaxation rate is expressed as[31]

$$k(t) \approx -\frac{d[\delta N(t)]/dt}{\delta N(0)}$$

$$= \frac{\langle \dot{G}; G(t) \rangle}{\langle G; G \rangle} = \frac{\int_0^\beta d\lambda \langle \dot{G}(-i\hbar\lambda)G(t) \rangle}{\beta \langle G; G \rangle}, \qquad (27)$$

where $G(t)$ is the Heisenberg operator of the function G and

$$\langle A; B \rangle = \frac{1}{\beta} \int_0^\beta d\lambda \, \text{Tr}[\exp(-\beta H)\exp(\lambda H)A$$
$$\times \exp(-\lambda H)B]/\text{Tr}[\exp(-\beta H)] \qquad (28)$$

is the canonical correlation for any two operators A and B. In the above, $\dot{G} = [G,H]/i\hbar$ and we may replace this by the Poisson bracket $\dot{G} = \{G,H\}$ in the classical limit $\hbar \to 0$. The trace operation in the canonical correlation reduce to an integral over the phase space, in this classical limit, and noncommutability of operators no longer plays a role. Thus we have

$$k(t) = \frac{\langle \{G,H\}G(\theta_t) \rangle}{\langle G; G \rangle} = \frac{\langle \dot{\theta}(dG/d\theta)G(\theta_t) \rangle}{\langle G \rangle}$$

$$= \frac{2\langle \dot{\theta}_t \delta(\theta_t - \pi)G(\theta) \rangle}{\langle G \rangle}, \qquad (29)$$

where $\langle \ \rangle$ now represents the thermal average over the phase space and the dynamics of θ_t and $\dot{\theta}_t$ follow the classical Liouville equation. To deduce the final equality, we used the fact that the terms including $\delta(\theta - \pi)$ and $-\delta(\theta - 2\pi)$ give the same contribution in this symmetric potential.

The initial value of the above rate has a very simple form[33]

$$k_{\text{TST}} \equiv k(0) = \frac{\langle |v_\theta| \delta(\theta - \pi) \rangle}{\langle G \rangle} = \langle |v_\theta| \rangle \frac{\langle \delta(\theta - \pi) \rangle}{\langle G \rangle}, \qquad (30)$$

where v_θ represents the velocity along θ. This can be computed without regard to the dynamics of the reactive event and gives the well-known transition state theory (TST) value.

The transformation of the correlation function (27) to the form (29) is particularly convenient in the classical limit because it immediately separates the problem into a part calculable by equilibrium theory [$k(0)$] and a correction calculable by importance sampling (trajectories start at the transition state). In the quantum regime, an analogous transformation has been made by Voth et al.[10] and is quite useful in path integral formulations. In the quantum kinetic equation formalism, these transformations do not seem as helpful and we have calculated rates by numerically carrying out the linear response experiment.

III. NUMERICAL RESULTS

A major goal of this study is to see the interplay of tunneling, resonance, and dissipation on a single potential; however, the change of population between the well via tunneling is extremely small in most "realistic" chemical reaction problems and it is time consuming to perform the numerical integration using present computers and calculation technique. So here we employ an ideal model where the tunneling processes play a dominant role to do a comprehensive study on reaction processes. The Hamiltonian of the reaction system itself is given by (hereafter $\hbar = 1$)

$$H_0 = \frac{\hat{P}^2}{2I} + U_0 \cos^2(\hat{\theta}) \quad (0 < \theta \leqslant 2\pi), \qquad (31)$$

where

$$I = 0.02, \quad U_0 = 40. \qquad (32)$$

We also suppressed the periodic boundary condition $W(P,0) = W(P,2\pi)$. The corresponding potential and its several eigenstates are illustrated in Fig. 2. This barrier is rather low for the description of the crossing as a strictly "activated event" at the higher temperature and low damping. However, it does allow the numerical illustration of the main phenomena through the range of possible motional parameters. As shown in this figure, the ground and the first
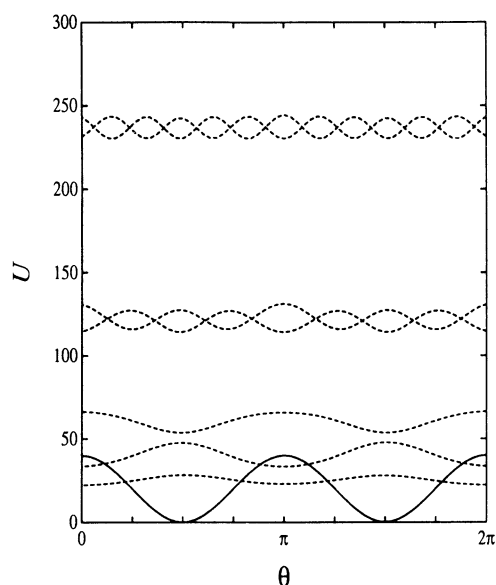
FIG. 2. The $\cos^2$ potential and its eigenstates and eigenvalues with the periodical boundary condition.
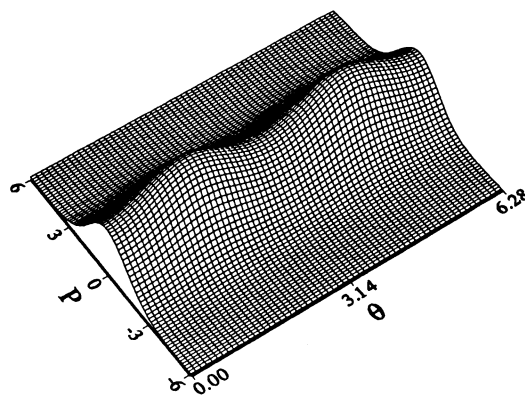
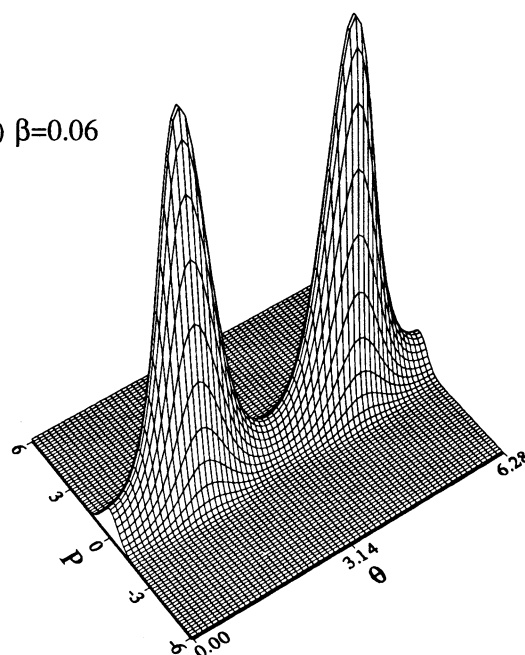(a) $\beta=0.01$

(b) $\beta=0.06$

FIG. 3. The classical equilibrium distribution function for the phase space for the $\cos^2$ potential at (a) the high temperature $\beta = 0.01$ and (b) at the low temperature $\beta = 0.06$.

excited states are in the potential. The fourth and the fifth, and sixth and seventh excited states are degenerate.

In this study, we mainly discuss the Gaussian-white cases based on the quantum Fokker–Planck equation (18) or the classical Fokker–Planck equation (19). The Gaussian–Markovian cases based on Eqs. (11)–(13) with the quantal Liouvillian [Eq. (15)], or the classical Liouvillian [Eq. (17)] are discussed at the end of this section. The numerical integrations of these kinetic equations were performed by using the second-order Runge–Kutta method for finite difference expressions of the momentum and the coordinate space (here we use 200×60 mesh). We use this mesh to simulate both the classical and the quantum reaction rates. We employed the center difference scheme for the differential operators in Eqs. (18) and (19). The discrete Fourier expression is used for the potential kernel (15) with Eq. (16).[28] The mesh we used is not very fine and the true reaction rates are somewhat lower than the reaction rates calculated here; however, the qualitative features of the activation processes are expected to be unchanged. In order to compare with the results from the simulation, we used the same mesh to compute the TST value [Eq. (30)]. The simulation was performed by following the procedure of the linear response experiment. In order to perform the numerical calculation, here we set $\epsilon = 0.005$ in Eq. (23).

A. Gaussian-white noise bath

Figures 3 and 4 show the equilibrium phase distribution at the different temperature calculated from the classical Fokker–Planck equation (19) and the quantum Fokker–Planck equation (18), respectively. At the high temperature, Figs. 3(a) and 4(a), the shapes of the population at the barrier top of the quantum result is larger than that of the classical one because of the tunneling contribution. In Fig. 4(b), the distribution function has negative parts, since the

distribution function for the quantum system (the Wigner function) is not positive definite. The shapes of the distribution functions for the quantum system depend on the coupling strength of the system–bath interaction and here these are shown for the weak interaction case $\zeta = 10$. The quantum distribution function for the strong coupling case will be discussed later.

Figures 5 and 6 show the time evolution of the quantum and the classical reaction rate functions, calculated from the classical Fokker–Planck and the quantum Fokker–Planck equations for various β. In these figures, the strength of the system–bath interaction is chosen to give $\zeta = 10$. First, we should note that since the mesh is finite, the results shown here are numerically inaccurate in the time period $t < 0.005$. If we exclude this error, the classical reaction rates (Fig. 6) start from TST values calculated from Eq. (30), whereas the quantum ones (Fig. 6) start from zero. In the classical case,
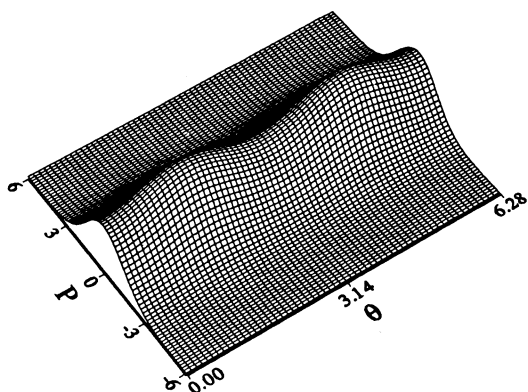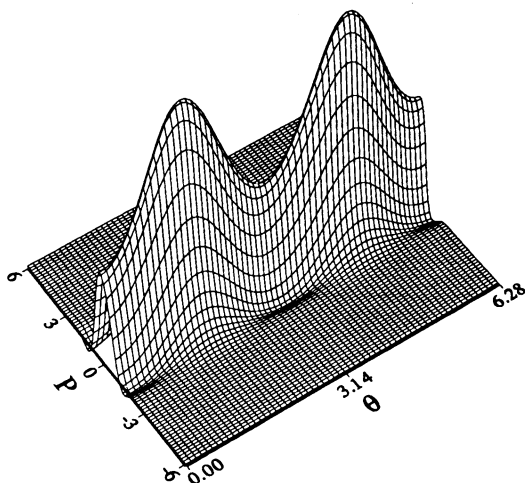
(a) β=0.01

(b) β=0.06

FIG. 4. The quantal equilibrium distribution for the phase space (the Wigner functions) at (a) $\beta = 0.01$ and (b) $\beta = 0.06$ for the weak interaction $\zeta = 10$.
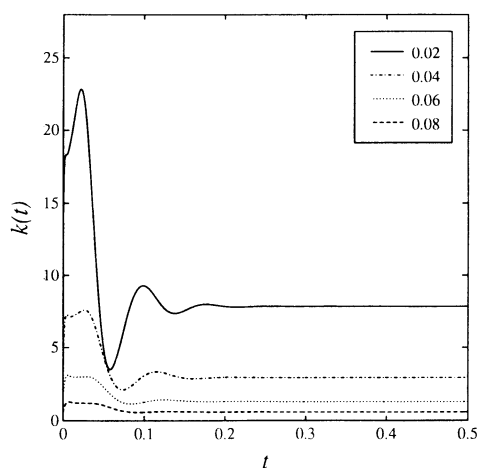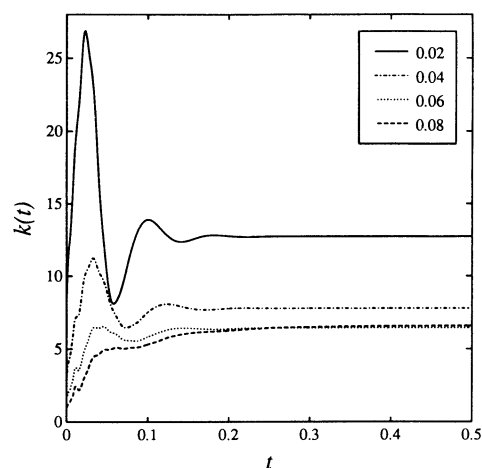

FIG. 6. Chemical reaction rates calculated from the quantum Fokker–Planck equation for different inverse temperature β for the weak interaction $\zeta = 10$.

FIG. 5. Chemical reaction rates calculated from the classical Fokker–Planck equation for different inverse temperature β for the weak interaction $\zeta = 10$.

the initial rates are determined by the free motion of the equilibrium molecules near the barrier top. In the quantum case, since quantum smearing of the transition state plays a role, the time-dependent reaction rates start from zero and then quickly rise up.[34] In both the classical and the quantum cases, since the potential is shallow, $\delta N(t)$ decreases rapidly at the initial stage and $k(t)$ increases until around $t = 0.05$. The reaction rates have oscillating features at high temperature until about $t = 0.02$ both in the classical and the quantum cases. In the classical case, this phenomenon is explained by recrossing caused by molecules that fail to get trapped, but in the quantum case, it is an interference phenomenon explained by the transition between the discrete eigenstates. Indeed, at the high temperature $\beta = 0.01$, the frequency of this oscillation is close to the transition energy between the ground state and the fourth or the fifth excited state, $\Delta\omega = 100$ (see Fig. 2). If temperature goes down, the oscillation frequency also decreases since the transition between the ground state and the lower excited states play more of a role. The rise time of the quantum reaction rates has a temperature dependence. Because of the interference of oscillating contributions from different levels, the rise is not simply $\beta\hbar$ in the quantum regime. After the rise time is over, the reaction rates quickly reach the plateau value (the relaxation value) at $t = 0.2$. When temperature goes down, this plateau value also falls in the classical case; however, because of the contribution from tunneling, the plateau values become constant at the low temperature in the quantum case.

Figure 7 shows TST values calculated from Eq. (30), together with the quantum and the classical relaxation rates for $\zeta = 10$ at the different temperature. As seen from the figure, the TST value and the classical relaxation value are exponential functions of β at low temperature, whereas the quantum relaxation value is temperature independent because of the tunneling contribution. At high temperatures $\beta = 0.01$–0.02, both the classical and TST values deviate slightly from the straight line. The source of deviation from
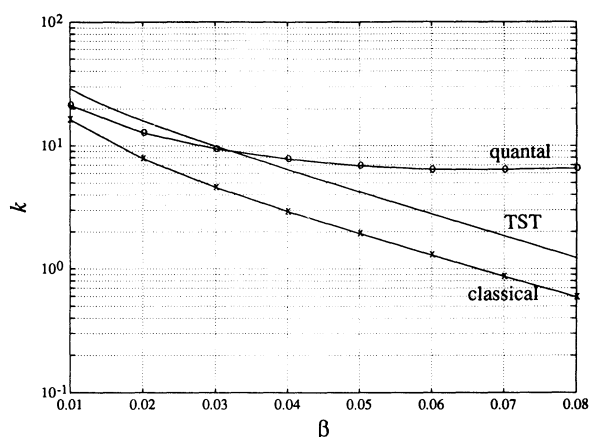
FIG. 7. Arrhenius plot of the TST, the classical relaxation, and the quantal relaxation values.

Arrhenius behavior here is the low barrier leading to large anharmonicity.

Figures 8 and 9 show the time evolution of the classical and the quantum distribution functions of θ at the low temperature $\beta = 0.06$ for the weak coupling $\zeta = 10$. Since the deviation of the distribution caused by the perturbation is so small, we plot
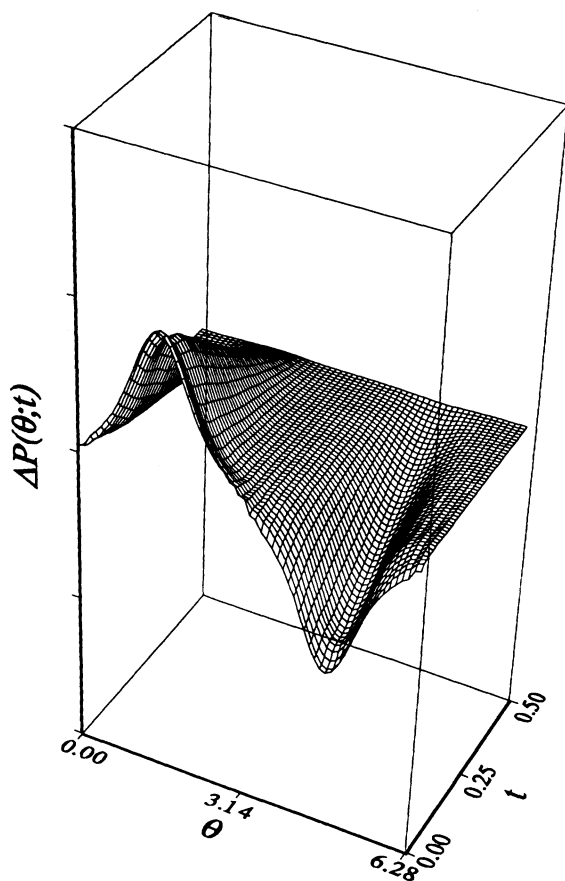

FIG. 9. Time evolution of the quantum distribution function. The parameters are the same as in Fig. 8.

$$\Delta P(\theta;t) \equiv P(\theta;t) - P(\theta;T)$$

$$= \int dp \, W(P,\theta;t) = \int dp \, W(P,\theta;T), \qquad (33)$$

where we set $T = 0.5$, instead of $P(\theta;t)$ itself. In the classical case, a slight change of the density operator at the top of the barrier $\theta = \pi$ can be observed; however, since the main contribution to the transition is from the tunneling process, the distribution function is smooth around the barrier top in the quantum case.

Figures 10 and 11 show the quantum and the classical reaction rates for different coupling strengths at (a) $\beta = 0.01$ and (b) $\beta = 0.06$, respectively. In the classical case (Fig. 10), the initial rates are determined by the free motion of the equilibrium molecules near the barrier top. For classical systems, the dissipation effect from the bath on these molecules does not change the probability of being at the transition state, thus graphs for different coupling strength start from the same initial value, which agrees with the TST values. Soon the molecules are scattered by the bath system through the interaction, or bounce off the side of the potential well. These effects lead to recrossing and a reduction in $k(t)$, as discussed in many papers. For weak interactions $\zeta = 10$ and 30, the bath ultimately provides a source of activation for the molecules and the rate constants increase with the coupling strength.[35] This is the energy controlled
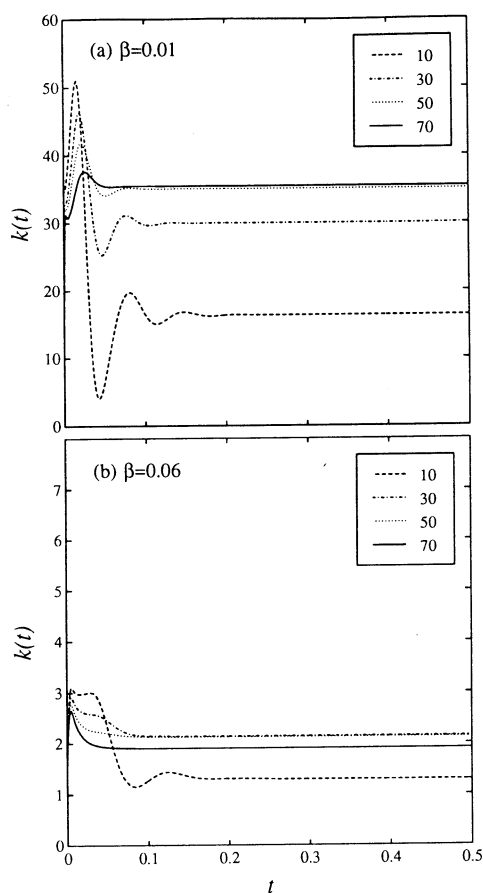

FIG. 8. Time evolution of the classical distribution function $P(\theta;t)$ at the low temperature $\beta = 0.06$ for the weak interaction $\zeta = 10$.

FIG. 10. Time evolution of the reaction rates calculated from the classical Fokker–Planck equation for various coupling strength ζ at (a) the high temperature $\beta = 0.01$ and (b) at the low temperature $\beta = 0.06$.
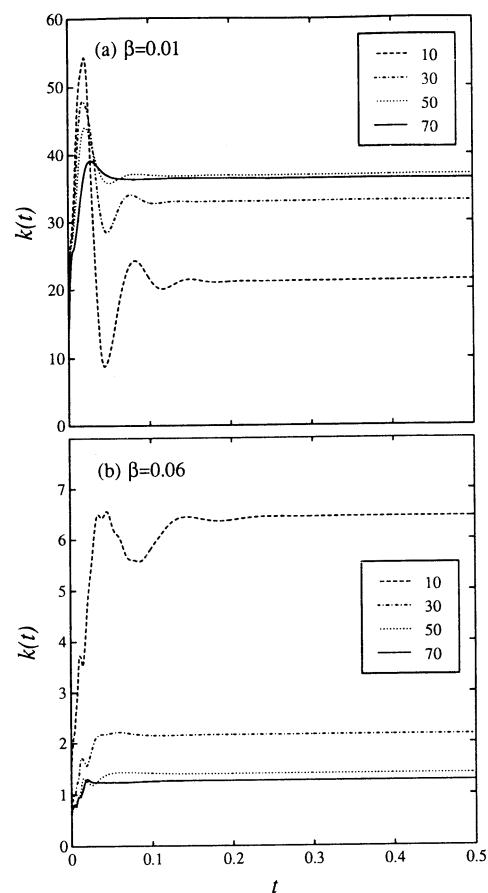

FIG. 11. Time evolution of the reaction rates calculated from the quantum Fokker–Planck equation. The other parameters are the same as in Fig. 10.

regime. However, for the strong interaction, molecules which have crossed the barrier may suffer collisions before reflecting from the potential well and reaction rates decrease with coupling strength. This is the diffusion limited regime and is observed at $\zeta = 70$ in Fig. 10(b). In Fig. 11(a), in the quantum case at the high temperature, the reaction rates show similar time evolution, except the initial point which is expected to be zero if mesh size is large enough. At low temperature [Fig. 11(b)], because of the tunneling, the reaction rates are much larger than the classical rates and oscillate slightly as shown in Fig. 6. If the interaction becomes stronger, this oscillation disappears and the plateau values become smaller. The reason for this is that the system–bath interaction suppresses the quantum effects and the phenomenon approaches the classical one. To illustrate this, we plot the plateau value vs coupling strength.

Figures 12 and 13 show the plateau value for different coupling strengths and temperatures. In Fig. 12, the turn-over feature from the energy controlled regime to the diffusion regime can be observed. These turning points shift to the right when the temperature goes down. The quantal results (Fig. 13) have a similar ζ dependence at high temperature. When temperature goes down, the contribution from the tunneling is revealed and shows a sharp peak around $\zeta = 5$. Some features of Fig. 13 may surprise the reader. Notice that

the rate is proportional to ζ; at small ζ even in the deep quantum regime. This is because k is defined by the asymptotic decay rate. At small ζ, populations oscillate for this symmetric situation and in that sense the phenomenology of rate law breaks down. The region of oscillating population is indicated by gray shading. The shape of the sharp peak in Fig. 13 does not appear to change even though the tempera-
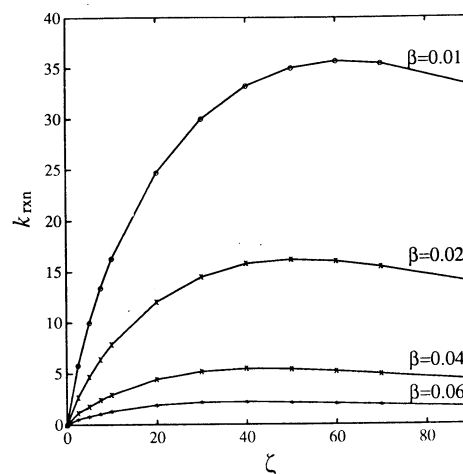

FIG. 12. The classical relaxation values are plotted as a function of the coupling strength at different inverse temperatures.
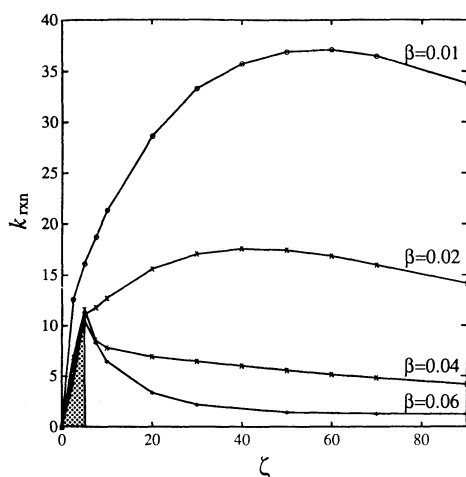
FIG. 13. The quantum relaxation values are plotted as a function of the coupling strength at different inverse temperatures.

ture goes down; however, shapes of graphs in the strong coupling region $\zeta > 20$ do change with the temperature and seem to approaching to the classical results in Fig. 12 as ζ is increased. To study these points, we plotted the quantum phase distribution for the strong interaction case at the low temperature in Fig. 14. Compared with Fig. 4(b), it is clear that the population around the barrier becomes smaller and the distribution functions approaches the classical one [Fig. 3(b)]. We may explain this phenomena from the equations of motion (18) and (19). As is well known, the equilibrium state for the classical Fokker–Planck equation is the Boltzmann distribution $W^e = \exp\{ - \beta[P^2/2m + U(\theta)]\}$ and satisfies

$$\hat{L}_{CL} W^e = 0, \quad \Gamma W^e \equiv \zeta \frac{\partial}{\partial P}\left(P + \frac{I}{\beta} \frac{\partial}{\partial P}\right) W^e = 0. \quad (34)$$

Since this eigenvalue of Γ is zero while the others are negative, Γ tries to force the distribution function to a Boltzmann one, but the potential term in Eq. (15) does not allow this form in the quantum case. However, if the interaction becomes very strong, the contribution of Γ becomes dominant and thus equilibrium distribution approaches to the classical one. Thus, we may conclude that the strong system–bath interaction suppresses the quantum effects on the system and the reaction rates approach the classical values if the interaction is very strong.

From the above discussion, the quantum reaction rate should always be larger than the classical one, although it becomes slightly smaller in the strong interaction case at $\beta = 0.06$ as seen in Figs. 12 and 13. This is attributed to the limitation of the quantum Fokker–Planck equation that the temperature of the bath should be very high or the system–bath interaction is weak. To improve upon this, we must take into account the low temperature corrections of Eq. (18) as shown in the Appendix of TW, or we must use the Fokker–Planck equation for the Gaussian–Markovian noise bath [Eqs. (11)–(13)], where the temperature limitation is weaker than the Gaussian-white case.

The major results of our paper are shown in Figs. 15 and 16. Here the relaxation values are plotted three dimensional-
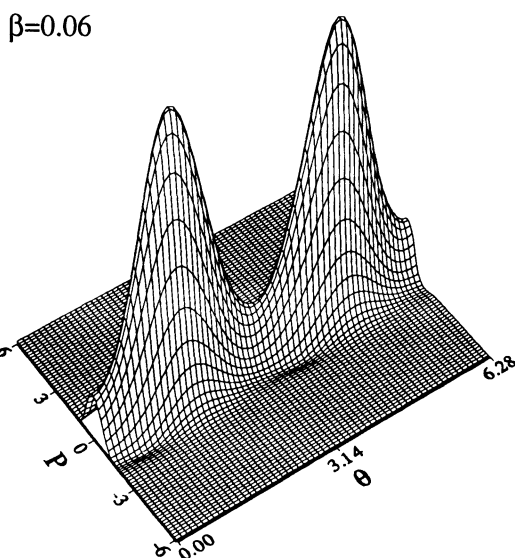
$\beta=0.06$

FIG. 14. The quantal equilibrium distribution for the phase space at $\beta = 0.06$ for the strong interaction $\zeta = 50$. The result for the weak interaction was shown in Fig. 4(b).
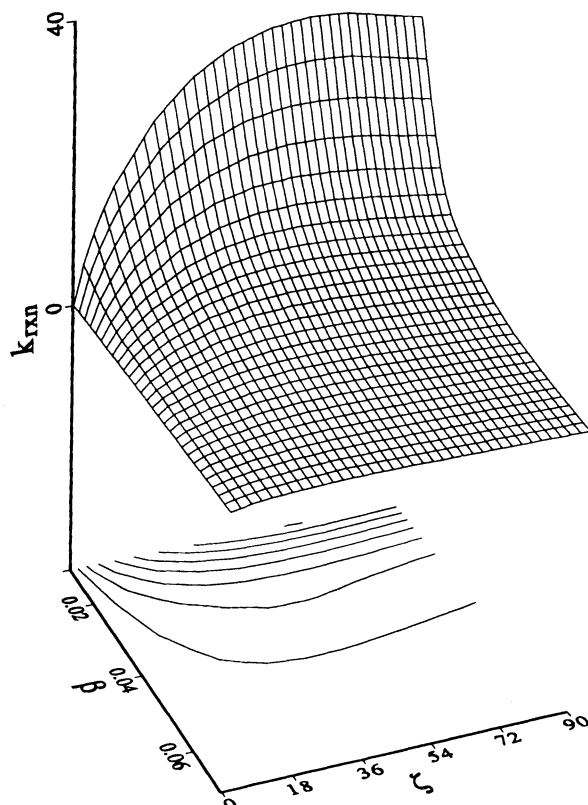

FIG. 15. The classical relaxation values are plotted as a function of the coupling strength and the inverse temperature. The lower graph shows the contour plot.
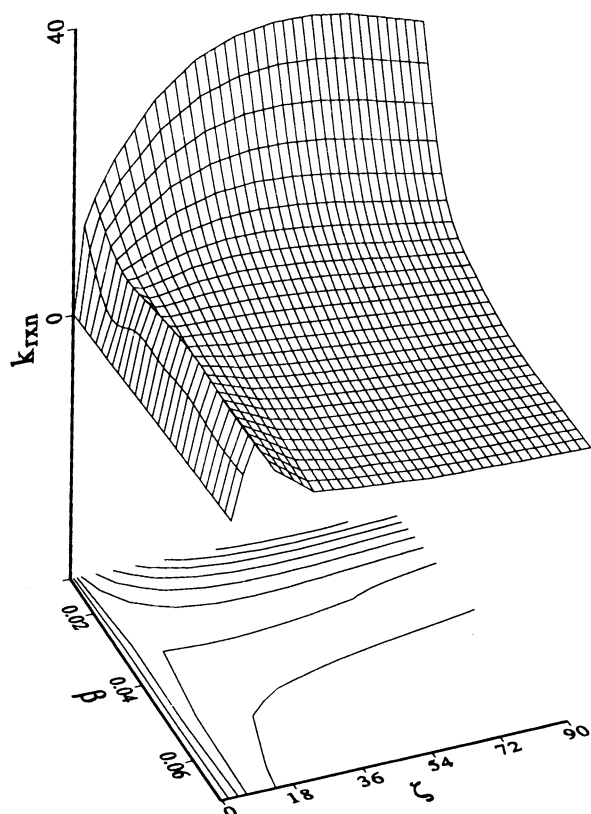
FIG. 16. The quantum relaxation values are plotted as a function of the coupling strength and the inverse temperature.

ly as a function of ζ and β going from the classical to the quantum regime as temperature is lowered. In Fig. 15, we see that the "Kramers turnover" shifts in the quantum regime. Figure 16 shows the onset of tunneling as temperature is lowered and the interplay of this with dissipation.

B. Gaussian–Markovian bath

In Fig. 17, we show the Gaussian–Markovian results at low temperature $\beta = 0.06$ calculated from Eqs. (11)–(13)
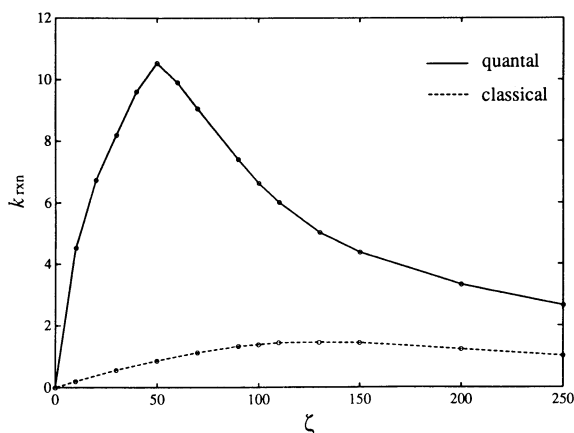

FIG. 17. The quantum and the classical relaxation rates calculated from the Fokker–Planck equation for the Gaussian–Markovian noise bath. The solid line represents the quantum result, whereas the dashed line represents the classical one.

with Eq. (15) in the quantum case and with Eq. (17) in the classical case. To perform the calculation, we decrease the mesh number from $N_P = 200$ to 50 keeping the same grid size. Since the distribution functions are localized at this low temperature, this does not change the results. We set $\gamma = 15$ and took into account about 40–120 hierarchy elements. As shown in Fig. 17, the ζ dependence of the reaction rate becomes weaker than the white noise. This is because the high-frequency oscillators of the bath no longer contribute to the damping in the Markovian case because of the frequency cutoff γ.

To see this point more clearly, we may introduce an effective coupling strength. Suppose that a phonon which has the same frequency as the characteristic frequency of the system ω_0 has the major contribution to the system–bath interaction. Because of the distribution equation (3), the coupling strength between this phonon and the system is

$$\zeta' = \frac{\zeta \gamma^2}{\gamma^2 + \omega_0^2}. \tag{35}$$

This is the effective coupling constant and we may set $\gamma \to \infty$ for Gaussian-white noise, while $\gamma = 15$ for Gaussian–Markovian noise. What characteristic frequency should be used? Here, we estimated as $\omega_0 \approx 50$ from the oscillations of the time-dependent reaction rate in Fig. 11(b) for the weak interaction at $\beta = 0.06$. In Fig. 18, we replot the Gaussian-white and Gaussian–Markovian results in the classical case and quantum case using this effective coupling strength as an abscissa. With this rescaling, the Gaussian–Markovian and Gaussian-white results now show a reasonable agreement for the weak interaction.
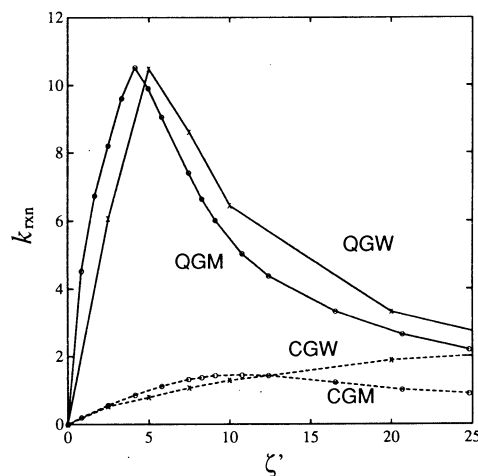

FIG. 18. The quantum and classical relaxation rates plotted vs effective coupling strength. The results calculated from the quantum Fokker–Planck equation (QGW), the classical Fokker–Planck equation (CGW), the quantum Fokker–Planck equation for the Gaussian–Markovian noise both (QGM), and the classical Fokker–Planck equation for the Gaussian–Markovian noise bath (CGM) are shown in the same graph. The solid lines represent the quantum results, whereas the dashed ones represent the classical results.

IV. PROSPECTS

Quantum kinetic equations can take advantage of modern grid-based numerical technology to study quantum barrier crossing over a wide range. With insights and some heroism, grid-based wave function methods have been extended to higher-dimensional problems.[36] The same should be true for problems with dissipation. The next stage of two-dimensional problems will already give some new insights, especially as to the interplay between internal energy relaxation and chaotic dynamics with various quantum effects. The extension of grid-based to much higher-dimensional systems becomes more difficult. Asymptotically, one can hope that clever Monte Carlo schemes, perhaps based on path integrals, will continue to materialize and that their numerical reliability can be explored. In the interim, numerical solutions of quantum kinetic equations can provide results that can be compared with qualitative ideas and approximate theories.

ACKNOWLEDGMENTS

[1]For reviews, see (a) P. Hänggi, P. Talkner, and M. Borkovec, Rev. Mod. Phys. **62**, 251 (1990); (b) J. N. Onuchic and P. G. Wolynes, J. Phys. Chem. **89**, 5852 (1988).

[2]D. Devault, *Quantum-Mechanical Tunnelling in Biological System*, 2nd ed. (Cambridge University, New York, 1984).

[3]R. P. Feynman and F. L. Vernon, Ann. Phys. (N.Y.) **24**, 118 (1963).

[4]A. O. Caldeira and A. J. Leggett, Ann. Phys. (N.Y.) **149**, 374 (1983).

[5]D. Chandler and P. G. Wolynes, J. Chem. Phys. **74**, 4078 (1981).

[6]J. D. Doll and D. L. Freeman, Science **234**, 1356 (1986).

[7](a) R. Jaquet and W. M. Miller, J. Chem. Phys. **89**, 2139 (1985); (b) K. Yamashita and W. H. Miller, *ibid.* **82**, 5475 (1985).

[8](a) A. Kuki and P. G. Wolynes, Science **236**, 1647 (1986); (b) P. G Wolynes, J. Chem. Phys. **87**, 6559 (1987).

[9]M. Gillan, J. Phys. C **20**, 3621 (1987).

[10](a) G. A. Voth, D. Chandler, and W. H. Miller, J. Phys. Chem. **93**, 7009 (1989); (b) J. Chem. Phys. **91**, 7749 (1989).

[11]C. Zheng, J. A. McCammon, and P. G. Wolynes, Proc. Natl. Acad. Sci. USA **86**, 6441 (1989).

[12]J. S. Bader, R. A. Kuharski, and D. Chandler, J. Phys. Chem. **93**, 230 (1990).

[13]C. Zheng, J. A. McCammon, and P. G. Wolynes, Chem. Phys. **158**, 261 (1991).

[14]V. Filinov, Nucl. Phys. B **271**, 717 (1986).

[15](a) N. Makri and W. H. Miller, Chem. Phys. Lett. **139**, 10 (1987); (b) J. Chem. Phys. **89**, 2170 (1988); (c) N. Makri, Chem. Phys. Lett. **159**, 489 (1989); (d) Comput. Phys. Commun. **63**, 389 (1991).

[16](a) J. D. Doll and D. L. Freeman, Adv. Chem. Phys. **73**, 120 (1988); (b) J. D. Doll, D. L. Freeman, and M. J. Gillan, Chem. Phys. Lett. **143**, 277 (1988); (c) J. D. Doll, T. L. Beck, and D. L. Freeman, J. Chem. Phys. **89**, 5753 (1988); (d) T. L. Beck, J. D. Doll, and D. L. Freeman, *ibid.* **90**, 3181 (1989).

[17](a) B. A. Mason, K. Hess, R. E. Cline, and P. G. Wolynes, Superlattices and Microstructures **3**, 421 (1987); (b) R. E. Cline and P. G. Wolynes, J. Chem. Phys. **88**, 4334 (1988).

[18]E. E. Nikitin, *Theory of Elementary Atomic and Molecular Processes in Gases* (Clarendon, Oxford, 1974).

[19]T. E. Bull, Chem. Phys. **143**, 381 (1990).

[20]J. M. Jean, G. R. Fleming, and R. A. Friesner, Ber. Bunsenges, Phys. Chem. **95**, 253 (1991).

[21]Y. Tanimura and R. Kubo, J. Phys. Soc. Jpn. **58**, 101 (1989).

[22]N. Makri, J. Chem. Phys. **94**, 4949 (1991).

[23]Y. Tanimura and P. G. Wolynes, Phys. Rev. A **43**, 4131 (1991).

[24]R. Kubo, M. Toda, and N. Hashitsume, *Statistical Physics* (Springer, New York, 1985), Vol. 2.

[25]A. O. Caldeira and A. J. Leggett, Phys. Status Solidi A **121**, 587 (1983).

[26]E. Wigner, Phys. Rev. **40**, 749 (1932).

[27]R. Kubo, J. Phys. Soc. Jpn. **19**, 2127 (1964).

[28]W. R. Frensley, Rev. Mod. Phys. **62**, 745 (1990).

[29]P. Pechukas, NATO ASI B **258**, *Proceedings of Large Scale Molecular Systems*, edited by W. Gans, A. Blumen, and A. Amann (Plenum, New York, 1991).

[30]V. Ambegaokar, Ber. Bunsenges. Phys. Chem. **95**, 400 (1991).

[31]T. Yamamoto, J. Chem. Phys. **33**, 281 (1960).

[32](a) W. H. Miller, J. Chem. Phys. **61**, 1823 (1974); (b) W. H. Miller, S. D. Schwartz, and J. W. Tromp, *ibid.* **79**, 4889 (1983).

[33](a) D. Chandler, J. Chem. Phys. **68**, 2959 (1978); (b) J. Montgomery, D. Chandler, and B. J. Berne, *ibid.* **70**, 4056, (1979); (c) J. Montgomery, S. L. Holmgren, and D. Chandler, *ibid.* **73**, 3688 (1980).

[34]J. Costley and P. Pechukas, Chem. Phys. Lett. **83**, 139 (1981).

[35]J. L. Skinner and P. G. Wolynes, J. Chem. Phys. **69**, 2143 (1978).

[36]See, e.g., (a) T. J. Park and J. C. Light, J. Chem. Phys. **88**, 4897 (1988); (b) J. Zhang and W. Miller, *ibid.* **88**, 4549 (1988); (c) M. D'Mello, C. Duneczky, and R. Wyatt, Chem. Phys. Lett. **148**, 169 (1988).